

RESEARCH ARTICLE

10.1002/2015JA021537

Special Section:

Variability of the Sun and Its Terrestrial Impact VarSITI

Key Points:

- Radiation belt substantially diminished during the prolonged solar minimum in 2009/2010
- This natural “Grand Experiment” allows us to test linkages between the belts and solar drivers
- Behavior is consistent with enhanced magnetospheric convection triggering whistler mode chorus

Correspondence to:

C. J. Rodger,
crodrger@physics.otago.ac.nz

Citation:

Rodger, C. J., K. Cresswell-Moorcock, and M. A. Clilverd (2016), Nature's Grand Experiment: Linkage between magnetospheric convection and the radiation belts, *J. Geophys. Res. Space Physics*, 121, 171–189, doi:10.1002/2015JA021537.

Received 4 JUN 2015

Accepted 14 NOV 2015

Accepted article online 18 NOV 2015

Published online 6 JAN 2016

Nature's Grand Experiment: Linkage between magnetospheric convection and the radiation belts

Craig J. Rodger¹, Kathy Cresswell-Moorcock¹, and Mark A. Clilverd²¹Department of Physics, University of Otago, Dunedin, New Zealand, ²British Antarctic Survey (NERC), Cambridge, UK

Abstract The solar minimum of 2007–2010 was unusually deep and long lived. In the later stages of this period the electron fluxes in the radiation belts dropped to extremely low levels. The flux of relativistic electrons (>1 MeV) was significantly diminished and at times was below instrument thresholds both for spacecraft located in geostationary orbits and also those in low-Earth orbit. This period has been described as a natural “Grand Experiment” allowing us to test our understanding of basic radiation belt physics and in particular the acceleration mechanisms which lead to enhancements in outer belt relativistic electron fluxes. Here we test the hypothesis that processes which initiate repetitive substorm onsets drive magnetospheric convection, which in turn triggers enhancement in whistler mode chorus that accelerates radiation belt electrons to relativistic energies. Conversely, individual substorms would not be associated with radiation belt acceleration. Contrasting observations from multiple satellites of energetic and relativistic electrons with substorm event lists, as well as chorus measurements, show that the data are consistent with the hypothesis. We show that repetitive substorms are associated with enhancements in the flux of energetic and relativistic electrons and enhanced whistler mode wave intensities. The enhancement in chorus wave power starts slightly before the repetitive substorm epoch onset. During the 2009/2010 period the only relativistic electron flux enhancements that occurred were preceded by repeated substorm onsets, consistent with enhanced magnetospheric convection as a trigger.

1. Introduction

The last solar minimum, which ended solar cycle 23, was unusually deep and long lived. Based on the timing of the last 4 solar minima, solar cycle 23 was expected to reach its minimum in 2006. However, the sunspot number and all other indicators of activity continued to drop throughout 2006–2008, with the minimum lasting to December 2009 [McDonald *et al.*, 2010]. The solar minimum exhibited properties that were “unprecedented in the space age” with solar wind and interplanetary conditions that had been “never seen” to date [Russell *et al.*, 2010]. As has been widely reported and discussed in the popular media, solar cycle 24 has continued to show low activity levels by the standards of recent history, confirming the predictions made by some [e.g., Svalgaard *et al.*, 2005; Clilverd *et al.*, 2006; Choudhuri *et al.*, 2007] but in stark contrast to other predictions [Dikpati *et al.*, 2006; Hathaway and Wilson, 2006].

The unusually quiet Sun in 2007–2010 resulted in lower values of the interplanetary magnetic field, and a slower approach of the tilt angle of the heliospheric current sheet toward the solar equator, than has been observed for recent solar minima [McDonald *et al.*, 2010]. This in turn led to a record of high level of measured galactic cosmic ray (GCR) intensity reported by ground-based neutron monitors [Zhao *et al.*, 2014] and spacecraft-measured intensities 20% higher than those in the previous solar minimum [Lave *et al.*, 2013]. These were the highest GCR intensities recorded during the space age. Due to the unusually long duration of the solar minimum, active research was undertaken into the significance of this solar minimum while it was ongoing. This effort produced a dedicated review article, submitted before the unusually deep minimum had finished [Russell *et al.*, 2010], which described the nature of the minimum and places it in the context of historical activity. The first figure of this review paper shows the changing flux of relativistic radiation belt electrons, with the outer belt “disappearing” during the very quiet period in early 2009 while there was also an extended period of low solar wind speeds. It is the link between solar activity and radiation belt electrons which will be the focus of the current study and in particular this time period.

The solar minimum between cycles 23 and 24 has been identified as an opportunity to better understand solar and solar-terrestrial physics, as it includes both extremely low activity levels and well-defined short-lived pulses of weaker activity which can be used to investigate the wider system response to a very well defined set of drivers. One example of this is the suggestion that this time period and the subsequent weak solar cycle 24 may provide an opportunity to “separate the climatic effects of solar and anthropogenic sources” [Russell et al., 2010]. During the Troitskaya-Cole Memorial Lecture at the 2011 International Union of Geodesy and Geophysics General Assembly, Daniel Baker referred to this time period as “Nature’s Grand Experiment” [Baker, 2011]. We have taken this phrase up for the title of this paper and wish to acknowledge his Plenary Lecture as the source.

There are still significant uncertainties about the source, loss, and transport of energetic electrons inside the Van Allen radiation belts [e.g., Reeves et al., 2009; Mauk et al., 2013; G. D. Reeves et al., 2013; Baker et al., 2015], despite the many decades which have passed since their discovery. The electrons in the outer belt may resonate with different magnetospheric waves, causing simultaneous changes in one or more of the electron’s momentum, pitch angle, or position which cause this belt to be highly dynamic [Thorne, 2010], with fluxes of energetic electrons changing by >3 orders of magnitude over time scales of hours to days [Li and Temerin, 2001; Morley et al., 2010].

It has long been recognized that high-speed solar wind stream (HSS) events are important drivers in major changes in the electron fluxes of the outer radiation belt [Paulikas and Blake, 1979; Reeves et al., 2011]. While the solar wind supplies the energy that drives the dynamics of the inner magnetosphere, the details of these mechanisms and their impact on the radiation belt are due to internal processes [Baker et al., 1989; Li et al., 1997], which are still under debate [Reeves et al., 2009]. For about the last 10 years there has been strong focus by the scientific community on the highly variable nature of the radiation belts [e.g., Millan and Baker, 2012; Mauk et al., 2013; G. D. Reeves et al., 2013]. This focus has led to a growing understanding of the many processes which can lead to the rapid acceleration and loss of outer radiation belt electrons, along with identification of the leading candidates driving the energization processes.

There is increasing evidence that a key player in the linkage between the solar wind and outer belt electron fluxes is the substorm. Substorms are a loading-unloading response that occurs when the interplanetary magnetic field (IMF) turns southward. During fast, geoeffective solar wind periods there is more frequent substorm activity [e.g., McPherron et al., 2009]. Enhancements in outer belt relativistic electron fluxes have been observed during times of prolonged substorm activity even in the absence of a geomagnetic storm [Meredith et al., 2003], with no significant flux enhancements seen unless the level of substorm activity was sufficiently high. An examination of HSS periods divided into southward IMF dominant HSS and northward IMF dominant HSS events found that on average the southward dominant HSS events produced relativistic electron flux enhancements [Miyoshi and Kataoka, 2008; McPherron et al., 2009]. These studies all identified the important role of whistler mode chorus waves in accelerating the electrons [e.g., Bortnik and Thorne, 2007; Thorne, 2010] to relativistic energies. Chorus waves are known to be strongly correlated with magnetospheric substorms [e.g., Tsurutani and Smith, 1974; Meredith et al., 2003]. Very recently, it has been demonstrated that acceleration by whistler mode chorus occurs during southward IMF dominant HSS events but that this mechanism is ineffective during HSS events with the northward IMF dominant [Miyoshi et al., 2013].

Investigations have been undertaken into the solar wind-magnetosphere coupling that leads to the enhanced chorus emissions and the subsequent electron flux enhancements. Lyons et al. [2005] found that relativistic electron energization occurs in association with large-amplitude Alfvén waves within the HSS that lead to intermittently large interplanetary magnetic field variations. These waves last for multiday periods causing multiday intervals in which there are intermittent periods of significantly enhanced magnetospheric convection followed by periods of weak convection. During the transition from strong convection to weak convection repetitive substorm onsets can occur. The enhanced convection of plasma sheet electrons toward the Earth increases their anisotropy, and energy flux, just outside the plasmapause, developing a region of enhanced chorus wave growth. The idea has been confirmed by Meredith et al. [2002] through the observation of intensified chorus waves and elevated plasma sheet fluxes in this region. The Lyons et al. [2005] study indicated that it is the periods of enhanced convection that precede substorm expansions, and not the expansions themselves, that lead to the enhanced dawnside chorus wave intensity. The importance of magnetospheric

convection in chorus wave growth and in determining electron flux enhancements has also been confirmed by *Kissinger et al.* [2014]. In addition, it has been shown that magnetospheric convection typically follows substorms and, in many cases, steady magnetospheric convection can be in the driven expansion or recovery phases of substorms [*Walach and Milan, 2015*].

In this paper we reexamine the impact of magnetospheric convection on outer belt energetic electron fluxes and the varying intensity of whistler mode chorus. We use repetitive substorm onsets as a proxy for enhanced convection conditions. Note that we assume that enhanced convection is driving the repetitive substorms, not that the convection is due to the substorms. However, it is possible that both statements are true; enhanced convection can arise from increased dayside reconnection as well as the nightside reconnection associated with substorms. Observations of energetic electrons from the multiple Polar-orbiting Operational Environmental Satellites (POES), Geostationary Operational Environmental Satellites (GOES), and also the Solar Anomalous and Magnetospheric Particle Explorer (SAMPEX) spacecraft are contrasted with whistler mode wave measurements from the Demeter satellite. Comparisons are made between time periods with repetitive substorm onsets that occur during HSS events and periods with isolated substorm events. Finally, we examine if the importance of magnetospheric convection occurring during repetitive substorms is consistent with the significant decreases in the relativistic outer radiation belt fluxes during Nature's Grand Experiment in 2009.

2. Experimental Data Sets

2.1. SAMPEX Observations

In July 1992 the Solar Anomalous and Magnetospheric Particle Explorer (SAMPEX) satellite was launched, reentering the atmosphere in late 2012 [*Baker et al., 2012*]. While the SAMPEX science mission officially ended in June 2004, operations continued throughout much of this time, with data available from the SAMPEX Data Center (<http://www.srl.caltech.edu/sampex/DataCenter>) and producing a large quantity of scientific results (see the overview by *Baker and Blake* [2012]). SAMPEX was in a low-Earth orbit with a period of ~ 96 min and an inclination of 81.7° [*Nakamura et al., 1998*]. The magnetic local time of the satellite repeated over ~ 80 days [*Blake et al., 1996*]. Because of the SAMPEX satellite's low-altitude polar orbit, it sampled the radiation belts ~ 60 times a day.

SAMPEX carried the Heavy Ion Large Telescope (HILT), which produced high sensitivity and high time resolution >1.05 MeV electron and >5 MeV proton flux measurements with an effective geometric factor of ~ 60 cm² sr [*Klecker et al., 1993*]. In the current study we use the HILT "Rate 5" datum which is the sum of the four Solid State Detector Rows and has a time resolution of 100 ms. All of the available HILT data at the SAMPEX Data Center from 1 January 1998 to the end of the data set on 3 November 2012 are included in our analysis. As an initial processing step we determine median HILT fluxes with 3 h time resolution and 0.25 International Geomagnetic Reference Field (IGRF) L shell resolution, having removed fluxes likely to be affected by the South Atlantic Magnetic Anomaly (SAMA) where there is typically significant proton contamination in low-Earth orbit particle data [e.g., *Rodger et al., 2013*]. As HILT responds to both electrons and protons, we also remove all data during solar proton events, where these events are defined using a highly conservative criterion as described below.

We utilize National Oceanic and Atmospheric Administration (NOAA) recorded and processed 5 min average >10 MeV proton flux observations from the GOES spacecraft as provided by the NASA High-Resolution OMNI data set, to identify periods where solar proton event contamination was likely to have occurred in our other data sets. *Cresswell-Moorcock et al.* [2015] noted that the D region of the upper atmosphere, at least, has the potential to respond to solar particle event (SPE) defining flux below the official threshold level of 10 pfu (where pfu is the >10 MeV proton flux unit (i.e., protons $\cdot s^{-1} sr^{-1} cm^{-2}$ at geostationary orbit)). We have taken their work as an indication that the commonly used 10 pfu threshold may not remove all SPE contamination. Therefore, we have applied a more conservative threshold, where a solar proton event time frame is defined as when the >10 MeV proton flux is above 1 pfu for three or more consecutive 5 min GOES observations.

2.2. POES Observations

The Polar-orbiting Operational Environmental Satellites (POES) are a set of low-altitude spacecraft (~ 800 – 850 km) in ~ 100 min period Sun-synchronous polar orbits. The POES spacecraft have carried the second

generation Space Environment Monitor (SEM-2) [Evans and Greer, 2004] since 1998. The SEM-2 Medium Energy Proton and Electron Detector monitors energetic charged-particle fluxes. At this point seven SEM-2 carrying POES spacecraft have flown (NOAA 15–19, MetOp 1 and 2). We will particularly focus on the SEM-2 integral electron telescopes observations. These telescopes point in two directions and have energies of >30 keV (e1), >100 keV (e2), and >300 keV (e3). One direction, labeled 90° , primarily measures trapped and drift loss cone electrons, while the 0° direction primarily measures deep inside the bounce loss cone [Rodger et al., 2010b, Appendix A]. It is well known that the POES SEM-2 suffers from significant proton contamination in the electron channels [Yando et al., 2011]. We correct this using an algorithm [Lam et al., 2010, Appendix A] which was recently validated by Whittaker et al. [2014]. In addition, we also exploit the P6 telescope which responds to relativistic electrons with energies above ~ 700 keV [Rodger et al., 2010a; Yando et al., 2011]. This can be used to monitor the variation in relativistic electron fluxes outside of time periods and locations where there is significant >6.9 MeV protons present. All the SEM-2 telescopes produce data integrated over 1 s, alternating every second between the 0° and 90° look directions.

We follow a similar initial processing outlined above for SAMPEX. Average fluxes are found using 0.25 IGRF L shell resolution having excluded observations in the SAMA and during solar proton events. Due to the high number of SEM-2 carrying satellites, we can move to a higher time resolution, in this case 15 min.

2.3. GOES Observations

We combine >2 MeV electron data (E2 channel) from multiple Geostationary Operational Environmental Satellites (GOES), to examine the time-varying relativistic electron fluxes at geostationary orbits. The data were downloaded from the NOAA National Geophysical Data Center, which has now been merged into the NOAA National Centers for Environmental Information. For GOES spacecraft numbered from 8 to 12 the observations were made by the Energetic Particle Sensor. For GOES spacecraft numbered 13 to 15 the observations were made by the Energetic Proton, Electron and Alpha Detectors. We used the 5 min averaged data files, as these include some correction for proton contamination in the electron channels, and also remove all data recorded during solar proton events.

2.4. Demeter Lower Band Chorus

We examine plasma wave activity using the ICE (Instrument Champ Electrique) instrument on board the Demeter spacecraft. Demeter was launched in June 2004 and was deorbited in March 2011. Demeter flew in a Sun-synchronous, 98° inclination orbit at an altitude of 670 km (after 2005). We analyze ICE/Demeter data up to early December 2010. The ICE instrument produced VLF band continuous power spectrum measurements of one electric field component [Berthelier et al., 2006]. We combine both Demeter burst and survey mode spectra. These have a frequency resolution of 19.25 Hz up to 20 kHz but were reprocessed at 0.25 L resolution to produce the hourly mean lower band chorus intensity (0.1–0.5 of the electron gyrofrequency) following the approach outlined in Neal et al. [2015]. It is important to note that below $L \sim 4$ the lower band chorus frequency band overlaps with that expected for plasmaspheric hiss (0.1–2 kHz [e.g., Meredith et al., 2004]), although this will only be significant inside the plasmapause.

2.5. SuperMAG Substorms

Identification of substorms can be challenging, and in some cases controversial, as different researchers focus upon different criteria with different instruments for their substorm definition. Here we use the substorm lists produced by SuperMAG [Gjerloev, 2012]. SuperMAG derives an AE -like index from more than 100 ground-based magnetometers. The onset of substorm expansion times is determined using SuperMAG observations by a validated automated algorithm [Newell and Gjerloev, 2011a, 2011b]. The events are available online from <http://supermag.jhuapl.edu/substorms/>. For the current study the SuperMAG substorm list was generated on 25 August 2014, 18:57:19 UT.

3. Cycle 23/24 Solar Minimum

In order to place the 2008/2009 time period of the “Grand Experiment” in context, we examine the long-term variations in radiation belt electron fluxes and other geophysical parameters.

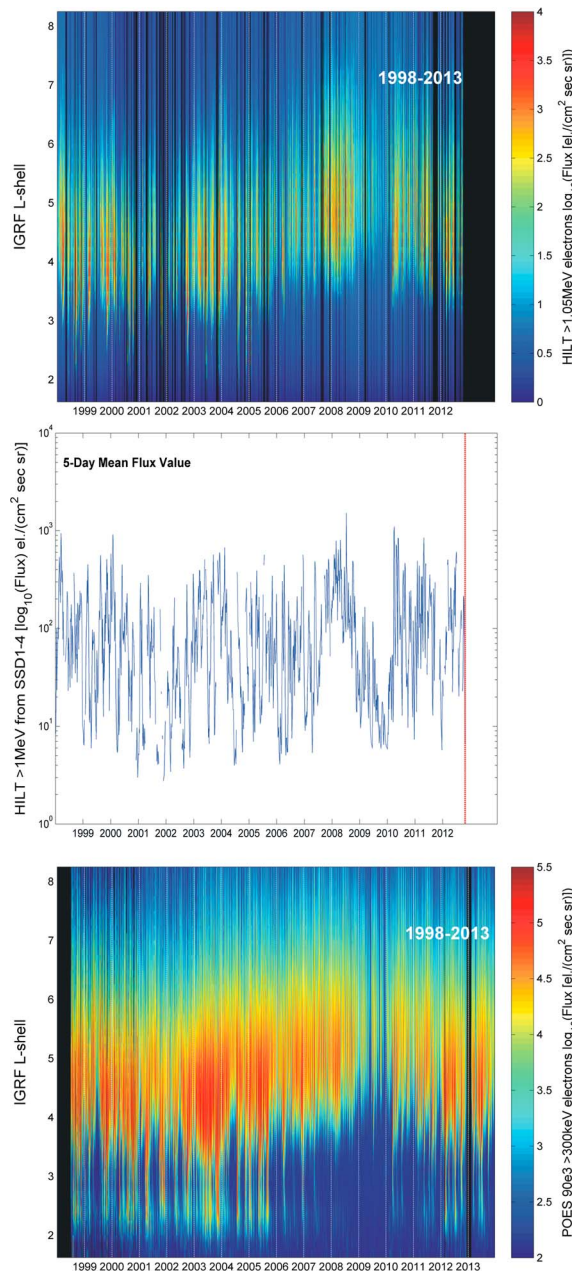


Figure 1. Variation of observed energetic electron fluxes across the time period 1998–2013. (top) The observations of >1.05 MeV SAMPEX HILT fluxes up to the end of the data set. (middle) The 5 day average fluxes from HILT across the outer radiation belt ($4 \leq L \leq 7$), where the red line marks the end of the HILT data set. (bottom) The POES-reported >300 keV fluxes from the 90° telescope.

observations” [Cresswell-Moorcock et al., 2013]. A plot of the 90P6 observations (not shown) strongly resembles that of SAMPEX in Figure 1, but with a smaller dynamic range due to the lower sensitivity of the SEM-2 to relativistic electrons. Figure 1 (bottom) shows the time variation of the POES SEM-2 >300 keV trapped electron fluxes as observed by the 90° telescope. Once again, the electron fluxes drop to very low levels in 2008/2009, standing out as a low activity period in the 15 years of data plotted. The late 2008 and 2009 quiet period clearly affected the radiation belt fluxes across a wide range of electron energies.

3.1. SAMPEX Observations

Figure 1 (top) shows the SAMPEX HILT >1.05 MeV fluxes from the start of 1998 to the end of 2013. The start and end dates of this plot are chosen for comparison with the POES SEM-2 observations. The end of the HILT data in late 2012 leads to the totally black region in the later part of the panel, while brief black regions are primarily caused by the removal of times with SPE occurring. As is clear from Figure 1 (top), the 2009 time period stands out as a particularly long period of low relativistic fluxes. This has been previously pointed out [Russell et al., 2010, Figure 1]. In addition, the SAMPEX summary paper commented “For all intents and purposes, the outer radiation belt disappeared entirely from November 2008 and all through 2009” [Baker and Blake, 2012, Figure 24].

Figure 1 (middle) shows the 5 day average fluxes observed by HILT across the outer radiation belt ($4 \leq L \leq 7$). A red vertical dashed line has been added to mark the end of the HILT data set. As can be seen in this figure there is typically a large range in the measured relativistic fluxes, but from late 2008 to 2009 the fluxes steadily decreased and then stayed at a very low level. The fluxes started to recover from mid-January 2010 and were strongly boosted at the start of April 2010.

3.2. POES Observations

It has previously been reported that decreases in the POES trapped relativistic electrons (90P6) occur in much the same way as reported by SAMPEX and seen in Figure 1 (top and middle). One study noted that changes in the 90P6 observations were “unprecedented in the ~14 years of SEM-2

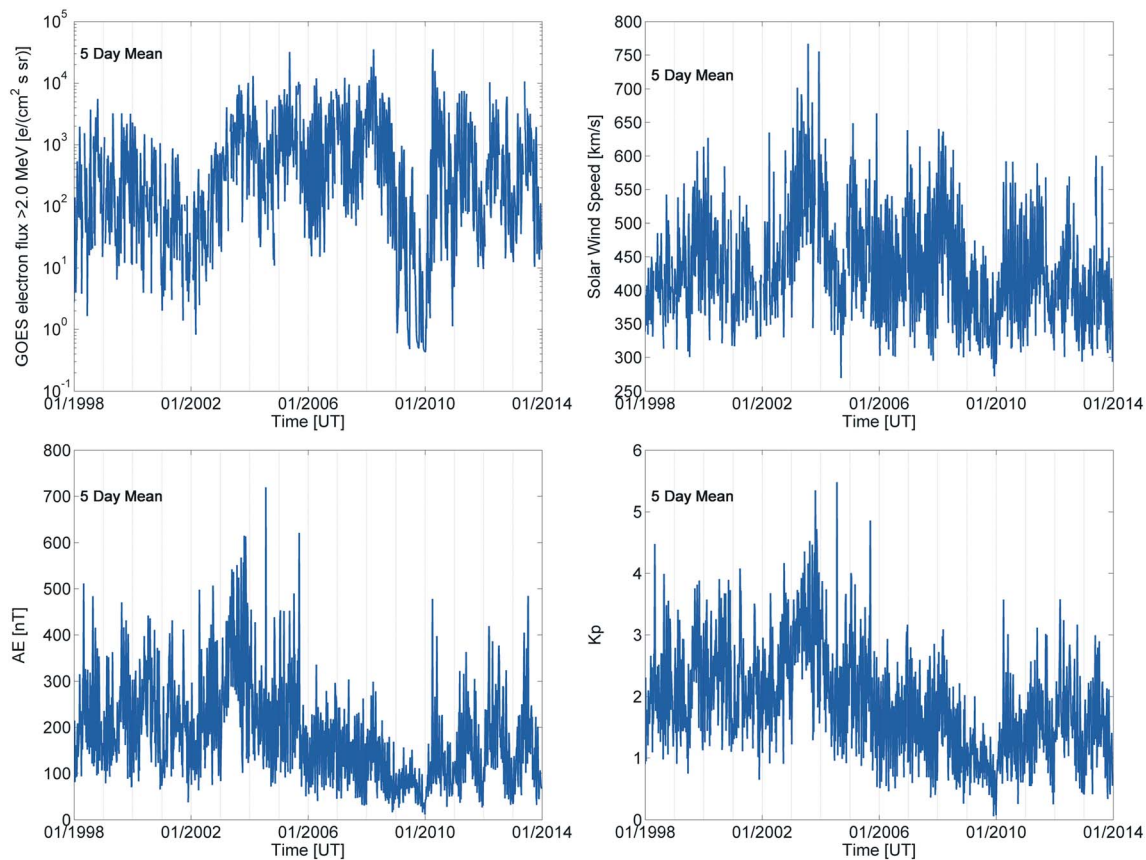


Figure 2. Long-term variation of multiple parameters across the time period shown in Figure 1. In all cases a 5 day mean is used to smooth the values. (top left) GOES measured >2 MeV electron fluxes. (top right) Solar wind speeds. Geomagnetic indices (bottom left) AE and (bottom right) Kp.

3.3. GOES Observations

The profound decrease in relativistic outer radiation belt electron fluxes also occurred at geostationary orbits. Figure 2 (top left) shows the long-term variation in GOES-observed >2 MeV electrons from the start of 1998 to the end of 2013, i.e., the same time periods as plotted in Figure 1. A 5 day mean is used to smooth the values and draw out the behavior. Once again, 2009 stands out as a long-lived period with extremely low fluxes. These observations are consistent with those reported from 1.8 to 3.5 MeV Los Alamos National Laboratory (LANL) geostationary electron fluxes [G. Reeves *et al.*, 2013], where it was found that during parts of 2009 the fluxes dropped below the instrument threshold. However, the LANL measurements also show that significant flux variations were observed during the prolonged solar minimum, such that the outer radiation belt did not disappear below measurement capabilities during the entirety of that period.

3.4. Demeter Observations

The variation in observed median Demeter lower band chorus wave power across its entire mission life has previously been reported [Neal *et al.*, 2015, Figure 3]. These authors also commented on decreased wave activity during the period of low energetic and relativistic fluxes, noting “Once again the solar minimum period in 2009 shows lower levels of chorus intensity, emphasizing the quietness of this time.” It appears that the 2009 period was typically 1–2 orders of magnitude lower in wave intensity than was normally seen.

3.5. Geophysical Parameters

Figure 2 shows the variation in a number of geophysical parameters across the same time period as plotted in Figure 1. In all cases a 5 day mean is used to smooth the values. Figure 2 (top right) shows the changing solar wind speed. From mid-November 2008 to late March 2010 the 5 day mean solar wind speed never reaches

higher than 475 km s^{-1} and only occasionally reaches values $>425 \text{ km s}^{-1}$. Note that the maximum solar wind speed value occurring during November 2008 to March 2010 depends on the averaging period. If one uses 1 day or 1 h averaging, the solar wind speed rarely exceeds 560 km s^{-1} . The average 5 day mean solar wind speed in 2009 is 368 km s^{-1} , to be contrasted with 430 km s^{-1} for the 1998–2013 period. A similar result was pointed out by *Russell et al.* [2010, Figure 1], although only considering up to the first few months of 2009, and by *Gibson et al.* [2011] who included data to the middle of 2010.

Figure 2 (bottom row) shows the variation in the geomagnetic indices *AE* (bottom left) and *Kp* (bottom right). The smoothed index values are consistently low across the period of interest. For example, over the entire time period plotted the mean *AE* is 182 nT, while it is only 70 nT in 2009, and the mean *Kp* for the entire period is 1.85 but only 0.9 in 2009. The variation of multiple geomagnetic indices across the prolonged minimum has also been examined previously [*Kilpua et al.*, 2014]. The year 2009 has also been used to investigate substorm occurrence and characteristics during quiet solar driving periods, showing that the recurrence times during very quiet solar wind-driving conditions are $\sim 5\text{--}8$ h, roughly double that of the average conditions [*Pulkkinen et al.*, 2014].

4. Superposed Epoch Selection

As noted in section 1, it has been suggested that convection occurring during repetitive substorms leads to an enhancement in dawnside chorus wave intensity, which energizes radiation belt electrons to relativistic energies. We test this concept using superposed epoch analysis of the POES SEM-2, SAMPEX HILT, and Demeter ICE observations. As many of our experimental measurements are contaminated during solar proton events, we remove epochs occurring during these times using the same criteria outlined in section 2.

4.1. Isolated and Recurrent Substorm Periods

The epochs are provided by the SuperMAG substorm event list, described in section 2.5, with the epoch selection criteria described below, following that suggested by *Newell and Gjerloev* [2011b]. These authors found that substorms do not have a preferred recurrence rate but rather fall into two distinct dynamic regimes, which they termed “isolated” and “recurrent.” The grouping into isolated and recurrent substorms [*Newell and Gjerloev*, 2011b] is conceptually the same as the random and quasiperiodic substorm groupings proposed by *Borovsky et al.* [1993]. We follow the *Newell and Gjerloev* naming convention, which was itself based on earlier terminology [*Kullen and Karlsson*, 2004; *Morley et al.*, 2009]. In addition, note that we take the recurrent substorm grouping to represent what multiple authors have previously referred to as “repetitive substorms” [e.g., *Lyons et al.*, 2005], what *Miyoshi and Kataoka* [2008] referred to as “continuous substorms,” and what *Cresswell-Moorcock et al.* [2013] referred to as “clustered substorms.”

We limit ourselves to considering substorms from 2005 to 2013. The choice of 2005 as the start date is to allow at least three POES SEM-2 satellites to be operating (NOAA 15–17), as this provides the appropriate level of spatial coverage required for our study. While Demeter operation ceased in December 2010 and SAMPEX in November 2012, we have produced epochs to 2013 to explore the conditions before and after 2009.

The definitions used in the current study are taken from those used by *Newell and Gjerloev* [2011b], which we summarize as follows.

Isolated substorm epoch. The event time for a substorm which is isolated in time from those surrounding it. These events have >3 h between them and both the closest previous event and the closest next event, such that the absolute time difference between events is $|\Delta T| > 3$ h.

Recurrent substorm epoch. The event time for the first substorm in a cluster of substorms which are closely spaced in time. The start of the cluster must be >82 min between it and any previous events. Each subsequent substorm in the chain must be spaced ≤ 82 min after its immediate previous neighbor. There is no restriction on the length of the recurrent substorm chain. The removal of substorm epochs occurring within our defined solar proton event times periods has the potential to move either the start or end of a chain of recurrent substorm epochs from its true time. However, this affected only 2 of the 2052 recurrent substorm epochs.

Table 1 provides a summary of the number of epochs and their annual variation from 2005 to 2013. Across this time period there were a total of 11,396 SuperMAG-detected substorms, i.e., an average of 1266 per year.

Table 1. Variation in the Number of SuperMAG-Reported Substorms by Year (SuperMAG All), As Well As the Number of Substorm-Defined Epochs Determined From the SuperMAG Substorm List^a

Substorm Type	All	2005	2006	2007	2008	2009	2010	2011	2012	2013
SuperMAG all	11,396	2,203	1,506	1,394	1,336	464	923	1,069	1,374	1,127
<i>After Solar Proton Events Removed</i>										
Isolated epochs	2,462	277	285	310	289	227	292	263	260	259
Recurrent epochs	2,052	374	300	316	307	73	157	173	181	171
Average #	2.9	3.0	2.8	2.8	2.7	2.3	3.1	2.6	3.0	3.0

^aThe criteria used to define the isolated and recurrent epochs are given in the text in section 4.1. The mean number of SuperMAG-reported substorms in each recurrent substorm chain is given in the last line of the table (Average #).

However, 2009 is clearly very different with only ~37% of the long-term average number. The lower section of Table 1 also shows the number of isolated and recurrent substorm epochs we employ in our superposed epoch analysis, after solar proton events are removed. Following the definitions described above, there are 2462 isolated substorm epochs (an average of 274/year) and 2052 recurrent substorm epochs (an average of 228/year). Typically, there are approximately three distinct SuperMAG-reported substorms in each recurrent substorm chain. Again, 2009 stands out as an unusual year, with ~17% fewer isolated substorm epochs, 68% fewer recurrent substorm epochs, and 0.6 less individual substorms on average occurring inside each recurrent chain.

4.2. Superposed Epoch Analysis of Substorms

Before examining the impact of these epochs on radiation belt fluxes and plasma waves, we first check the superposed epoch analysis of these epochs for solar wind parameters and the AU and Kp geomagnetic indices. Figure 3 presents the results of the superposed epoch analysis showing the typical behavior of the IMF B_z , solar wind speed, AU , and Kp values for both the isolated (left column) and recurrent (right column) substorm epochs. In all panels in this figure the superposed epoch median of the plotted parameter is given by the solid black line and the 95% confidence interval for this median is shown by the red band. The dark blue bands mark the interquartile range and the 95% confidence interval about it (lighter blue).

As expected, in both cases the variation in the IMF B_z (first row) shows a strong, sharp, southward turning at the substorm epoch time. Consistent with the literature [e.g., McPherron *et al.*, 2009], substorm events occurring in periods of HSS fit the definition of recurrent substorms, while isolated substorms tend to occur during comparatively low solar wind speeds (second row). Finally, isolated substorm epochs occur during quiet geomagnetic conditions as defined by AU and Kp , while recurrent substorm epochs tend to occur during somewhat disturbed geomagnetic times (third and fourth rows). Note that Kp is a good measure of convection [Thomsen, 2004], as is the AU index [e.g., Weimer, 1994]. The variability shown in Figure 3 (third and fourth rows) suggests more convection during the times of the recurrent substorm epochs, starting before the zero epoch time.

5. Effect on Radiation Belt Fluxes

Figure 4 presents the results of superposed epoch analysis of the energetic and relativistic trapped electrons measured by the POES SEM-2 90° directed telescope. We consider the precipitating electrons in Appendix A. Figure 4 (first row) repeats the solar wind speed superposed epoch analysis from Figure 3 to provide context. Figure 4 (second to fourth rows) shows the POES trapped electron flux variations against IGRF L shell and time relative to the isolated (left column) and recurrent (right column) substorm epochs. In all cases medians are utilized in the analysis to ensure that the response is not dominated by rare extreme events. As is clear from this figure, there is only a small response in the trapped electron population at the times of the isolated substorm epochs. In all panels there is a small short-lived transient increase in the outer radiation belt fluxes, lasting approximately ~3 h and starting at the epoch time, which is most probably caused by the direct injection of some electrons into trapped and quasi-trapped pitch angles. Due to the short time scale, this effect is hard to see in Figure 4. Approximately 0.75 days after the isolated substorm epoch, there is an ~35–50% increase in the >100 and >300 keV fluxes, peaking about 1 day after the epoch and decaying to background levels about 3 days after the epoch. Even for the comparatively low solar wind speeds associated with the times of the isolated substorm epochs, there is a consistent, but small, response in the trapped outer radiation belt energetic and relativistic electron fluxes.

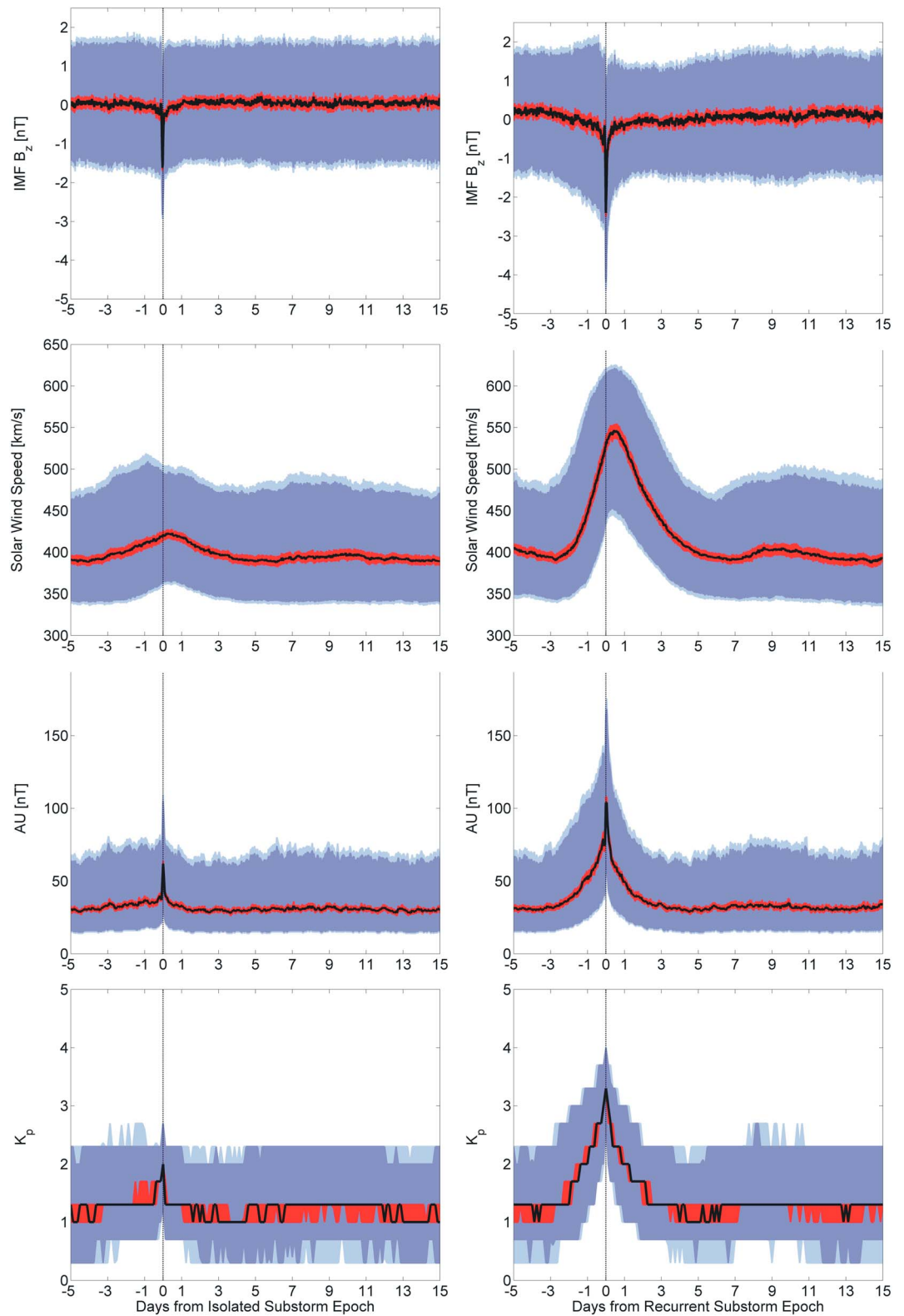


Figure 3. Results of the superposed epoch analysis showing the typical behavior of the IMF B_z , solar wind speed, AU, and K_p values for (left column) isolated and (right column) recurrent substorm epochs. The zero epoch time is marked by a thin vertical line at zero. In all cases the superposed epoch median of the plotted parameter is given by the solid black line. The 95% confidence interval for this median is shown by the red band. The dark blue bands mark the interquartile range and the 95% confidence interval about it (light blue).

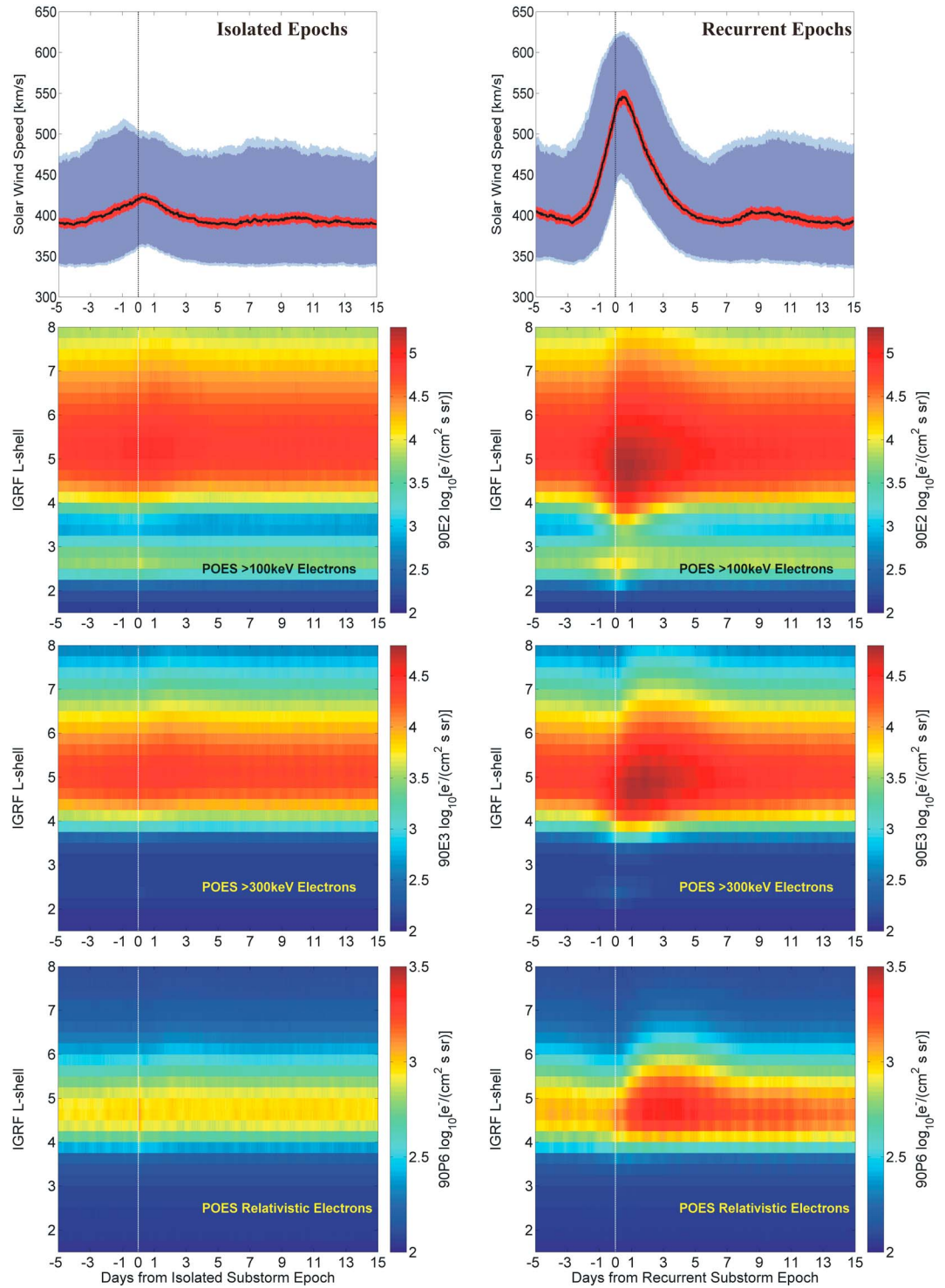


Figure 4. Superposed epoch analysis of median POES trapped electrons from the 90° detector for the (left column) isolated and (right column) recurrent substorm epochs, plotted against IGRF L shell. (first row) The solar wind speed superposed epoch analysis for context, in the same format as Figure 3. (second row) The >100 keV (e2) channel, (third row) the >300 keV (e3), and (fourth row) relativistic electrons from the P6 detector.

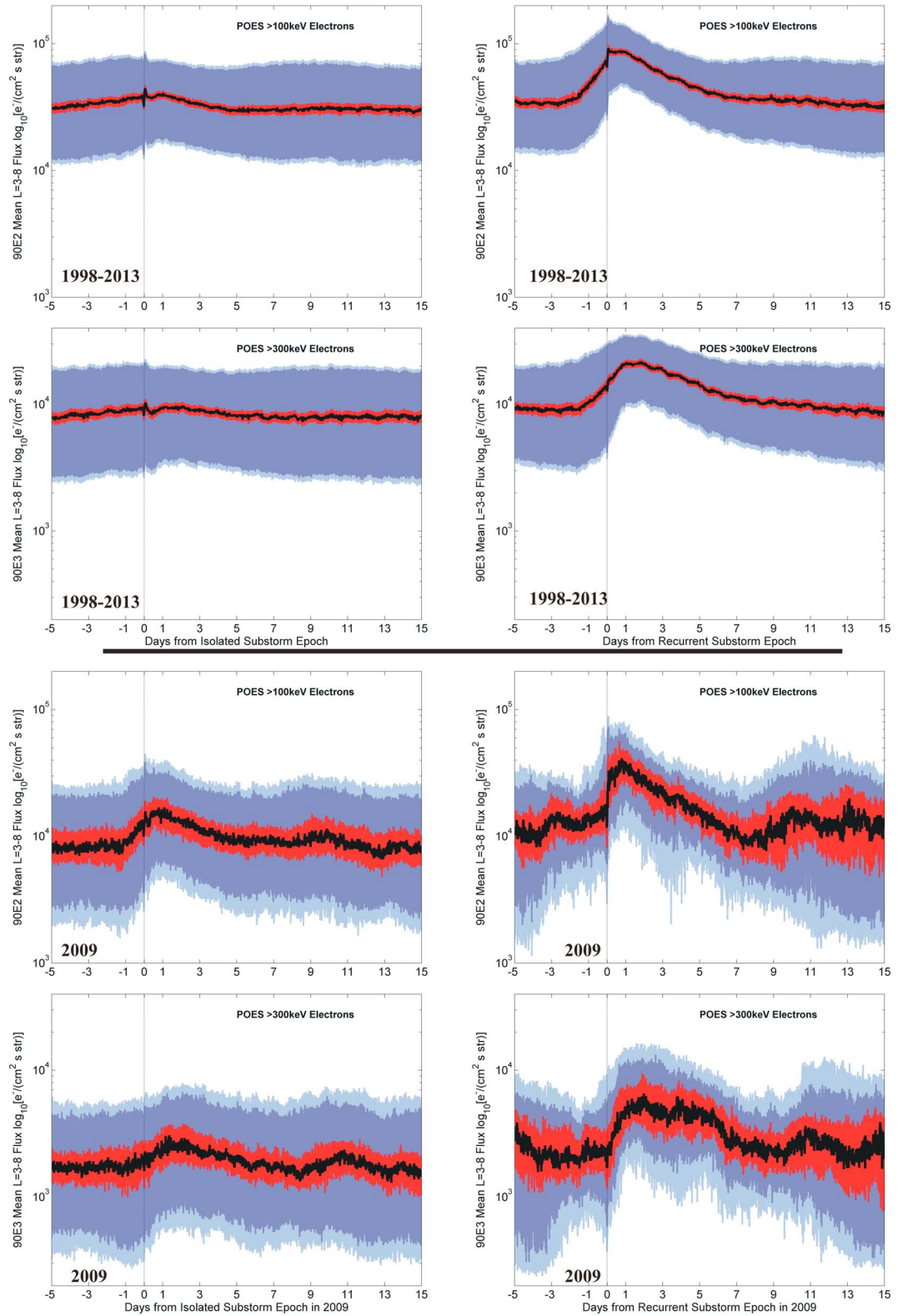


Figure 5. Superposed epoch analysis of mean $L = 3-8$ POES trapped >100 and >300 keV electron fluxes for the (left column) isolated and (right column) recurrent substorm epochs. Epochs spanning (first and second rows) the period 1998–2013 and (third and fourth rows) period restricted to 2009 only. The colors are consistent with those used in Figure 3.

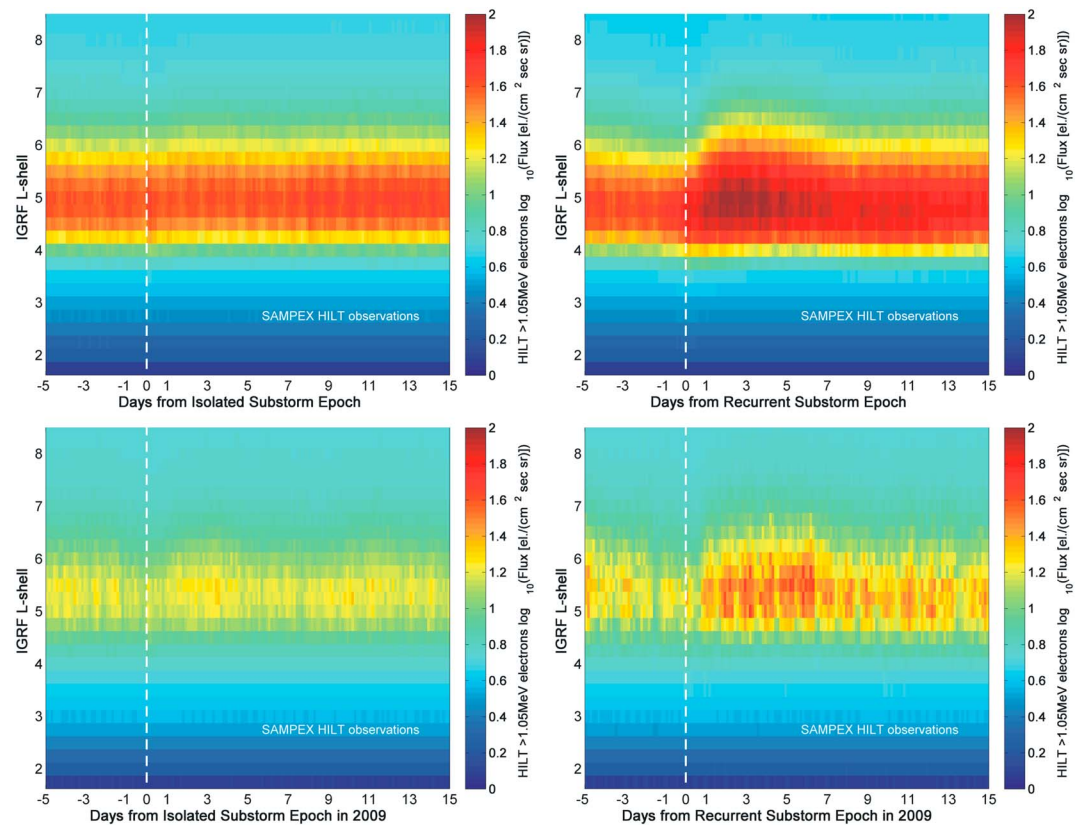


Figure 6. Superposed epoch analysis of the SAMPEX HILT >1.05 MeV trapped electron flux observations. All epochs (top row) across 1998–2013 and (bottom row) restricted to 2009 only.

In contrast, the response of the trapped electron fluxes at recurrent substorm epochs is far clearer. In this case there is evidence of progressive acceleration of electrons, with the >100 keV flux enhancement peaking at ~0.75 days after the zero epoch, >300 keV at ~2 days, and the P6 relativistic electrons peaking at ~3 days. The typical median peak enhancement is a factor of 3 in all of the energy channels.

Figure 5 shows a line plot representation of the changes shown in Figure 4. Here a “radiation belt index” is determined by finding the mean trapped flux from $L = 3–8$ and then undertaking the superposed epoch analysis as described above. The colors used in Figure 5 have the same meaning as in Figure 3. Figure 5 (first and second rows) shows the superposed epoch analysis for the >100 keV and >300 keV trapped fluxes for all the epochs from 1998 to 2013, i.e., the same epochs for Figure 4. In this case the short-lived transient changes at epoch time can be seen. These panels also show that there is a highly consistent change in the trapped fluxes after increases in magnetospheric convection, seen through the proxy of recurrent substorm epochs.

We have repeated the superposed epoch analysis shown in Figure 4 on the relativistic electrons measured by the SAMPEX HILT instrument. This is shown in Figure 6 in essentially the same format as Figure 4 (second to fourth rows). Again, the >1.05 MeV relativistic electrons show very little response to the isolated substorm epochs but have a factor of ~3 enhancement for recurrent substorm epochs at an L value of ~4.8.

6. Effect on Whistler Mode Chorus

As noted earlier it has been suggested that the acceleration of the outer belt electrons may be caused by whistler mode chorus. We test this hypothesis by examining the variation in lower band chorus following the same approach we took in section 5. Figure 7 shows the results of the superposed epoch analysis on Demeter measurements of lower band chorus wave power. This is plotted against L shell. In this case we

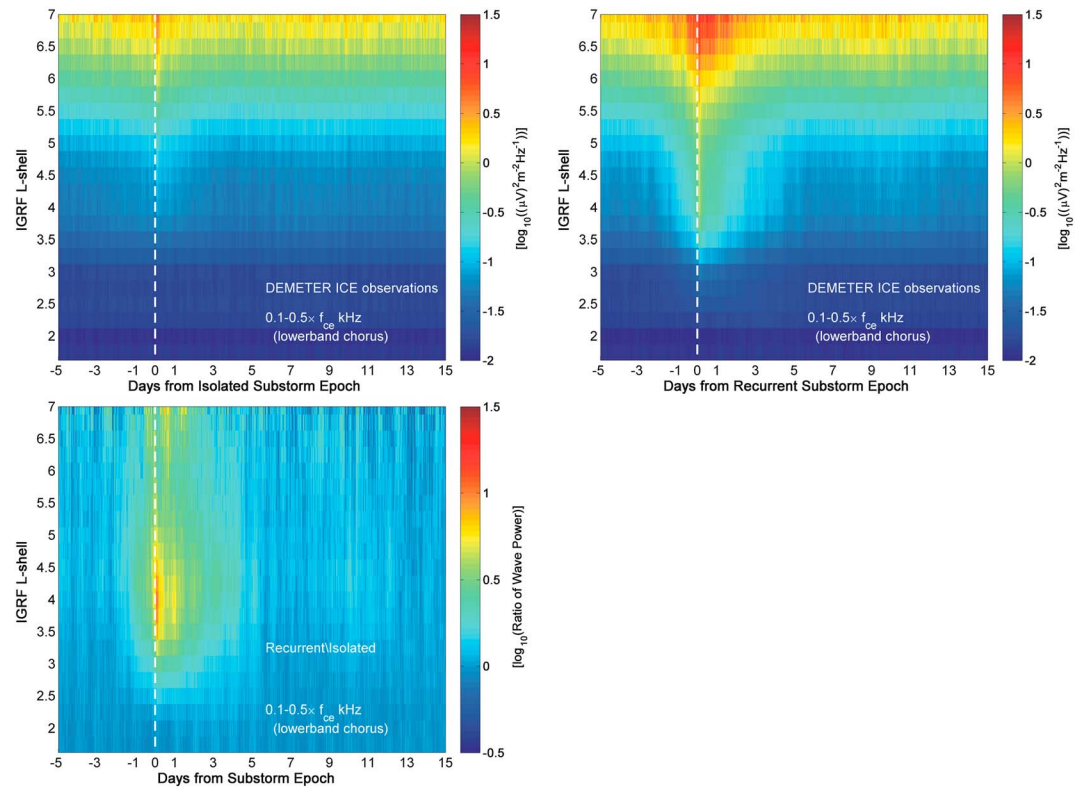


Figure 7. Superposed epoch analysis of the Demeter lower band chorus wave power observations for the (top left) isolated and (top right) recurrent substorm epochs. (bottom) The ratio of Figure 7 (top right and top left).

do not consider the chorus power variation beyond $L = 7$, as the number of Demeter observations is too low in this range. As before the isolated (top left) and recurrent (top right) substorm epochs are plotted separately in Figure 7 (top row). Figure 7 (bottom) shows the ratio of Figure 7 (top row).

In the case of the isolated substorm epochs there is a small increase in lower band chorus wave power, starting shortly after the epoch (about ~ 1 h) and peaking 2 h after the epoch. At this time the wave power is ~ 3 times higher than the background levels. In contrast, for recurrent substorm epochs there is a factor of ~ 4 increase in the lower band chorus wave power with a slow rise from background levels starting ~ 2 days before the epoch to reach this level ~ 6 h before the epoch and a factor of ~ 13 increase relative to the background levels spiking at 2 h after the epoch. The factor of 4 increase lasts about 1 day and then decays to reach background levels around 4 days after the epoch.

It is the combination of the different time response and the increased enhancements in whistler mode chorus which leads to the pattern seen in the ratio plot of the wave power shown in Figure 7 (bottom). While from ~ 1.5 days before the epoch there is a small increase in chorus intensities in the recurrent substorm epochs relative to the isolated substorm epochs, there is also a rapid additional enhancement which starts 4 h before the epoch with wave powers 3 to ~ 11 times larger, peaking ~ 2 h after the substorm epoch. The ratio of the isolated and recurrent wave power returns to unity ~ 5.5 days after the zero epoch, indicating that there is almost a weeklong period in which lower band chorus is enhanced and an ~ 4.5 day period during which the wave powers are at least doubled.

These observations are consistent with the concept that the differing behavior of whistler mode chorus can explain the different responses in the trapped electron fluxes. There is significantly more chorus power present during periods in which enhanced convection is expected using recurrent substorm epochs as a proxy. The periods with enhanced convection are associated with significantly more energetic and relativistic electron acceleration. In addition, as suggested by *Lyons et al.* [2005] there is a significant increase in the chorus activity shortly before the proxy epoch, which would be consistent with the important role played by increased magnetospheric convection in enhancing whistler mode chorus.

7. Reexamining the 2009 Period

Our analysis suggests that significant acceleration of outer radiation belt electrons tends to occur in association with recurrent substorms, most likely caused by magnetospheric convection enhancing the whistler mode chorus intensities. We now return to the 2009/2010 time period of the Grand Experiment. We have examined the superposed epoch analysis for solar wind parameters and the AU and Kp geomagnetic indices shown in Figure 3 but now restricted only to epochs occurring in 2009 (not shown). While there is more scatter in the behavior than seen in Figure 3, the 2009 restricted response is similar in all parameters but generally less pronounced. The AU median change at the zero epoch is slightly smaller in 2009 than for the complete epoch list, with a peak median value of 45 nT and 65 nT for the isolated and recurrent substorm epochs and zero epoch median Kp values of 1.7 and 2.7, respectively. The zero epoch median solar wind speed values are also smaller than shown in Figure 3, at 390 km/s for isolated substorm epochs and 440 km/s for recurrent substorm epochs. While the 2009 responses are smaller, the AU and Kp behavior still indicates the presence of increased magnetospheric convection at the times of the recurrent substorm epochs.

Superposed epoch analysis of the L -varying trapped POES fluxes, as shown in Figure 4 but now restricted to only 2009 epochs (not shown), indicates that there are distinct increases in the trapped fluxes after periods of increased magnetospheric convection, but these are not as strong as those seen in Figure 4. Evidence for this can be seen in Figure 5 (third and fourth rows), which are line plots of the superposed epoch analysis of the mean trapped POES fluxes restricted to 2009 epochs. In contrast with Figure 5 (first and second rows), the initial flux levels are lower, and the enhancements are also lower, consistent with smaller levels of enhanced convection. Figure 6 (bottom row) shows the SAMPEX HILT relativistic flux superposed epoch analysis restricted only to epochs in 2009. While the intensity of the responses is smaller, the same behavior is seen in 2009 as for the longer time period. We have also examined the variation in lower band chorus from DEMETER for the 2009 epochs (not shown). The response is not as clear as shown in Figure 7, but there is a general increase in chorus power from ~ 1 day before the recurrent substorm epochs. This analysis suggests that while the inner magnetosphere was less strongly driven in the 2009 time period, it is responding in a similar manner.

We now consider whether we can identify differences in the response of the outer radiation belt to increased convection on a case by case basis, using substorm epochs in 2009 as a proxy. Figure 8 presents the relativistic flux changes which occurred between 1 April 2009 and 31 December 2009, from SAMPEX HILT (top) and POES P6 (middle). The timing of recurrent substorm epochs has been overplotted by white vertical lines, while the times of isolated substorm epochs are shown with green crosses near the bottom of the panels. The daily summed number of substorms making up the recurrent substorm epochs is shown as white circles in Figure 8 (top and middle), while the daily number of isolated substorm epochs is shown as green circles. Figure 8 (bottom) shows the variation in outer radiation belt ($L = 3-6$) Demeter-observed lower band chorus power across this time. The blue line is the 1 h resolution median wave power, while the red and yellow lines in this panel are 2 day mean and median smoothing, respectively. These mean and median smoothed values are very similar, so the mean is somewhat obscured. This figure indicates that during time periods where no recurrent substorm epochs occurred, the fluxes steadily decrease, consistent with the lack of magnetospheric convection enhanced plasma wave activity. Throughout those time periods there are multiple isolated substorm epochs (with one to three isolated substorms per day), including time periods where the fluxes have dropped below the sensitivity of either of the electron flux-measuring instruments. In contrast, the majority of recurrent substorm epochs are associated with increases in the outer radiation belt relativistic flux. It is, however, not clear that there is a strong correlation between the intensity of the flux increase and the daily number of summed substorms present inside a recurrent chain. Figure 8 contains examples of periods where multiple recurrent substorm epochs occur, and there is little detectable response in the relativistic fluxes (e.g., October and November 2009). Together, these factors suggest that the recurrent substorms are not a sufficient condition for acceleration to take place, emphasizing the complexity of the system.

8. Discussion

The work presented here appears to support the work by others [e.g., Lyons *et al.*, 2005] suggesting the important role of magnetospheric convection in triggering the processes which lead to acceleration of

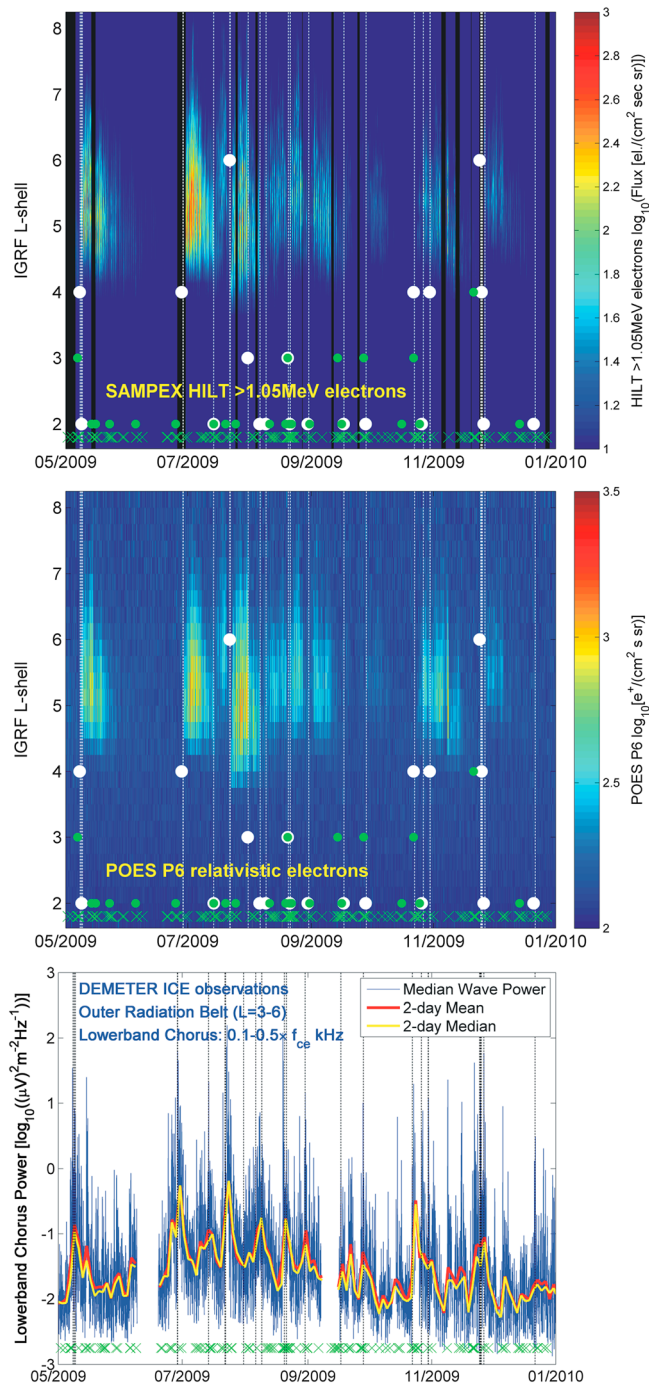


Figure 8. Variation of (top) SAMPEX HILT >1.05 MeV electrons, (middle) relativistic electrons from POES P6, and (bottom) Demeter lower band chorus power focused on the time of Nature’s Grand Experiment. The onset time of the recurrent substorm epochs is marked with vertical dashed lines, while the times of isolated substorm epochs are shown with green crosses. The daily summed number of substorms making up the recurrent substorm epochs is shown as white circles and the number of isolated substorm epochs per day as green circles. Figure 8 (bottom) shows the variation in lower band chorus power across $L = 3–6$. The black sections of Figure 8 (top) and white in Figure 8 (bottom) are caused by missing data.

radiation belt electrons and enhancements in the trapped energetic electron flux in the outer radiation belt. It has also identified the value in examining events in 2009 as a natural laboratory for testing our understanding of inner magnetospheric physics. However, it is not entirely clear from the results presented here that we have conclusively shown the value of focusing upon the Grand Experiment period relative to the longer data

set. The responses in Figure 5 for 2009 (third and fourth rows) are similar to those for the entire time period (first and second rows), except that the responses are weaker. Our analysis in Figure 8 is highly suggestive that 2009 should be a useful period to test our knowledge of magnetospheric physics, which might be confirmed by future modeling studies.

We acknowledge that this study could be extended into the examination of other parameters and that future research in this area would be worthwhile. In our study we have limited ourselves to electron flux and plasma wave observations from low-Earth orbiting spacecraft, but note that there would likely be value in examining measurements made closer to the geomagnetic equator. For example, in the current study we have employed substorms as a proxy for magnetospheric convection. There would clearly be value in investigating other measures for magnetospheric convection, either through different proxies or more direct measures. One approach would be to investigate the importance of convection using *AU* rather than substorms as a proxy, which should allow a more quantitative examination between the convection strength and the flux and wave enhancements. Finally, it is worth noting that the Lyons *et al.* [2005] study suggested that the enhanced magnetospheric convection was due to large-amplitude Alfvén waves within the HSS. We suggest that future studies should examine the presence of such waves in the solar wind as a more direct indicator of the linkages reported in the current study.

The 2009 period was anomalously quiet, allowing a better chance to disentangle the complex and interlinked processes. While our results are consistent with radiation belt acceleration due to enhanced convection (proxied through substorms), it is possible that they may also be consistent with other acceleration mechanisms, for example, solar wind-driven magnetospheric ULF wave [e.g., Kepko *et al.*, 2002; Pokhotelov *et al.*, 2015]. This deserves further examination.

9. Summary and Conclusions

In this paper we have examined the impact of repetitive substorm onsets on outer belt energetic electron fluxes and the varying intensity of whistler mode chorus. Making use of observations from multiple spacecraft, we have shown that these repetitive substorms are associated with enhancements in the flux of energetic and relativistic electrons, most probably due to enhanced whistler mode wave intensities which occur around the time of the start of the chain of substorms. The enhancement in chorus wave power starts slightly before the substorms start, consistent with earlier findings that strong magnetospheric convection beginning before repetitive substorm activity drives the chorus wave enhancement which accelerates the electrons.

We have also considered if this set of interconnected physical processes might explain the variation in relativistic outer radiation belt fluxes during Nature's Grand Experiment in 2009/2010. In that time period there were generally very low flux levels, with only short-lived pulses of enhanced fluxes. We find that all the enhanced relativistic fluxes in Figure 8 correspond to time periods immediately after repetitive substorm periods, consistent with enhanced magnetospheric convection as a trigger for acceleration. However, there are also some examples in this figure of recurrent substorm epochs when there is only a weak enhancement in lower band chorus power and no associated radiation belt enhancement. We suggest that the recurrent substorms are not a sufficient condition for radiation belt flux enhancement; however, enhanced convection (for which the substorms are only a proxy) and the subsequent wave growth may provide the necessary conditions.

Appendix A: Precipitation During Substorm Events

The current paper focuses on the linkages between substorms, whistler mode chorus, and trapped outer radiation belt electrons. In recent years there has been additional interest in energetic electron precipitation into the upper atmosphere [e.g., Cresswell-Moorcock *et al.*, 2013; Beharrell *et al.*, 2015], in part due to the connection to high-latitude polar atmospheric chemistry [e.g., Andersson *et al.*, 2012, 2014]. It has also been reported that the precipitation from substorms in 2009 was weaker than when compared with other years [Cresswell-Moorcock *et al.*, 2013]. Those authors noted that "the substorms in 2009 are largely isolated events, separated in time by many hours, while in 2010 substorms tend to occur in short-lived clusters associated with periods of enhanced solar wind speeds."

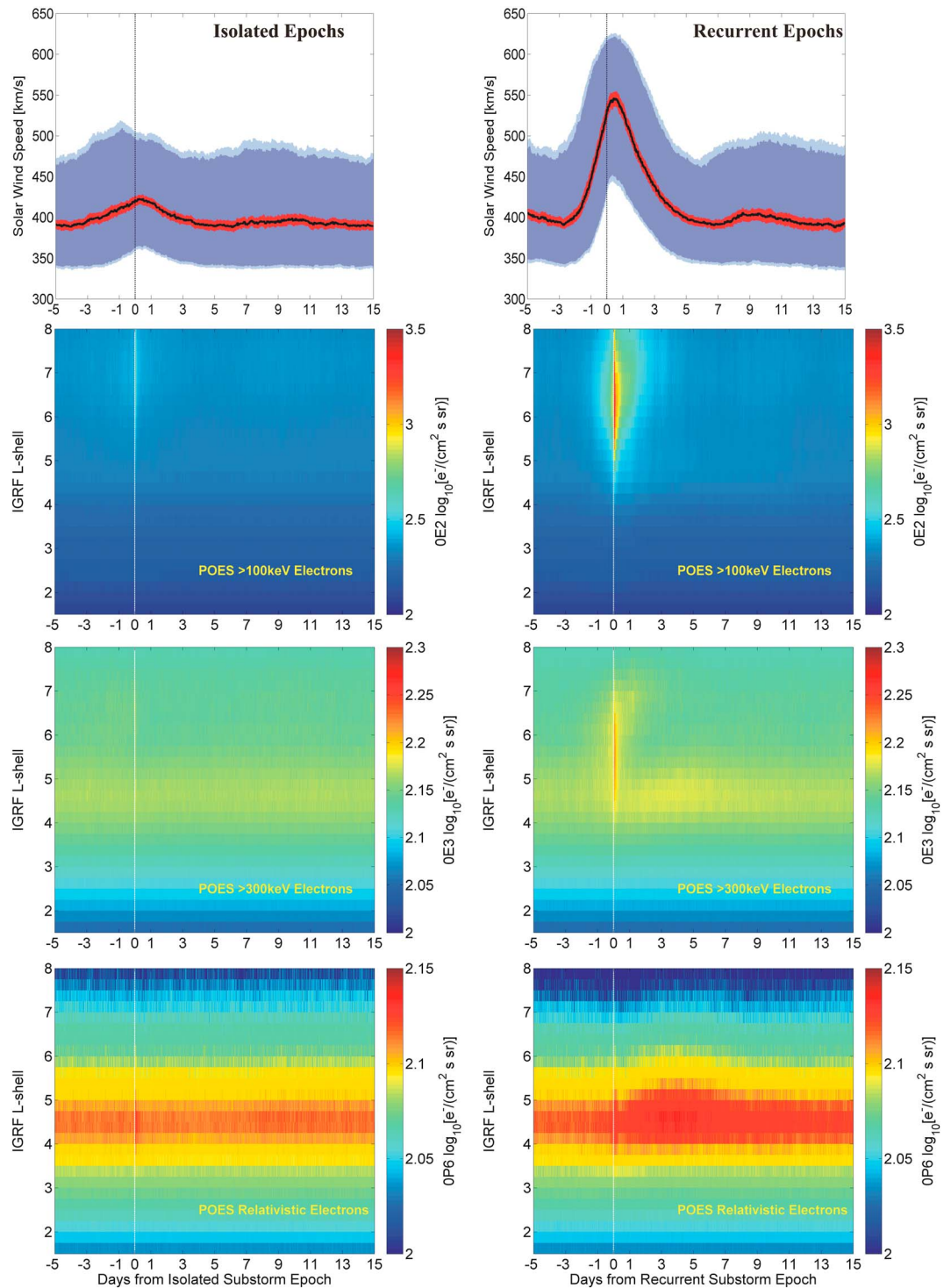


Figure A1. Superposed epoch analysis of median POES precipitation electrons from the 0° detector for the (left column) isolated and (right column) recurrent substorm epochs, plotted against IGRF L shell. The figure is otherwise in the same format as Figure 4.

Figure A1 presents the results of the superposed epoch analysis for the POES-detected precipitating electrons from the 0° detector, in the same format as Figure 4. For isolated substorms the precipitation is enhanced, but the enhancement is small relative to the POES SEM-2 noise floor flux of $\sim 100 \text{ cm}^{-2} \text{ s}^{-1} \text{ sr}^{-1}$. The precipitation starts immediately after the epoch time and lasts ~ 3 h in all three panels. In contrast, the

energetic electron precipitation for the recurrent substorm epochs shows about an order of magnitude higher peak fluxes for the >100 keV and >300 keV electrons peaking immediately after the epoch time, typically located at higher L shells and lasting ~ 3 days (albeit at very low levels). In addition, there is a small increase in >300 keV and relativistic electrons ~ 4 days after the recurrent substorm zero epoch in outer radiation belt L shells.

Acknowledgments

The authors would like to thank the researchers and engineers of NOAA's Space Environment Center for the provision of the data and the operation of the SEM-2 instrument carried on board these spacecraft and the many individuals involved in the operation of SAMPEX over 20 years. K.C.-M. was supported by the University of Otago via Summer Studentship and a PhD scholarship. For the SuperMAG substorm lists we gratefully acknowledge the following: Intermagnet; USGS, Jeffrey J. Love; CARISMA, PI Ian Mann; CANMOS; the S-RAMP database, PI K. Yumoto, and K. Shiokawa; the SPIDR database; AARI, PI Oleg Troshichev; the MACCS program, PI M. Engebretson, Geomagnetism Unit of the Geological Survey of Canada; GIMA; MEASURE, UCLA IGPP, and Florida Institute of Technology; SAMBA, PI Eftyhia Zesta; 210 Chain, PI K. Yumoto; SAMNET, PI Farideh Honary; the institutes who maintain the IMAGE magnetometer array, PI Eija Tanskanen; PENGUIN; AUTUMN, PI Martin Connors; DTU Space, PI Jürgen Matzka; South Pole and McMurdo Magnetometer, Pls Louis J. Lanzarotti and Alan T. Weatherwax; ICESTAR; RAPIDMAG; PENGUIN; British Antarctic Survey; McMac, PI Peter Chi; BGS, PI Susan Macmillan; Pushkov Institute of Terrestrial Magnetism, Ionosphere and Radio Wave Propagation (IZMIRAN); GFZ, PI Jürgen Matzka; MFGI, PI B. Heilig; IGFAPAS, PI J. Reda; University of L'Aquila, PI M. Vellante; and SuperMAG, PI Jesper W. Gjerloev. For the GOES and POES data we acknowledge the Space Weather Prediction Center, Boulder, CO, National Oceanic and Atmospheric Administration (NOAA), U.S. Department of Commerce. Data availability is described at the following websites: <http://www.srl.caltech.edu/sampex/DataCenter/index.html> (SAMPEX), <http://satdat.ngdc.noaa.gov/sem/poes/data/> (POES SEM-2), <http://Demeter.cnrs-orleans.fr/> (Demeter) and <http://supermag.jhuapl.edu/substorm/> (SuperMAG), wdc.kugi.kyoto-u.ac.jp (AE and Kp), http://spdf.gsfc.nasa.gov/pub/data/omni/high_res_omni/monthly_1min/ (solar wind speed), http://spdf.gsfc.nasa.gov/pub/data/omni/high_res_omni/ (GOES protons), and http://satdat.ngdc.noaa.gov/sem/goes/data/new_avg/YYYY/MM/goesXX/csv/ (GOES electrons).

References

- Andersson, M., P. T. Verronen, C. J. Rodger, M. A. Clilverd, and A. Seppälä (2014), Missing link in the Sun-climate connection: Long-term effect of energetic electron precipitation on mesospheric ozone, *Nat. Commun.*, doi:10.1038/ncomms6197.
- Andersson, M. E., P. T. Verronen, S. Wang, C. J. Rodger, M. A. Clilverd, and B. R. Carson (2012), Precipitating radiation belt electrons and enhancements of mesospheric hydroxyl during 2004–2009, *J. Geophys. Res.*, *117*, D09304, doi:10.1029/2011JD017246.
- Baker, D. (2011), *Assessing Solar and Solar-Terrestrial Influences as a Component of Earth's Climate Change Picture*, IUGG Program Handbook, p. 32, Int. Union of Geod. and Geophys., Melbourne, Victoria.
- Baker, D. N., and J. B. Blake (2012), SAMPEX: A long-serving radiation belt sentinel, in *Dynamics of the Earth's Radiation Belts and Inner Magnetosphere*, edited by D. Summers et al., AGU, Washington, D. C., doi:10.1029/2012GM001368.
- Baker, D. N., J. B. Blake, L. B. Callis, R. D. Belian, and T. E. Cayton (1989), Relativistic electrons near geostationary orbit: Evidence for internal magnetospheric acceleration, *Geophys. Res. Lett.*, *16*(6), 559–562, doi:10.1029/GL016i006p00559.
- Baker, D. N., J. E. Mazur, and G. Mason (2012), SAMPEX to reenter atmosphere: Twenty-year mission will end, *Space Weather*, *10*, S05006, doi:10.1029/2012SW000804.
- Baker, D. N., et al. (2015), An impenetrable barrier to ultrarelativistic electrons in the Van Allen radiation belts, *Nature*, *515*, 531–534, doi:10.1038/nature13956.
- Beharrell, M. J., F. Honary, C. J. Rodger, and M. A. Clilverd (2015), Substorm-induced energetic electron precipitation: Morphology and prediction, *J. Geophys. Res. Space Physics*, *120*, 2993–3008, doi:10.1002/2014JA020632.
- Blake, J. B., M. D. Looper, D. N. Baker, R. Nakamura, B. Klecker, and D. Hovestadt (1996), New high temporal and spatial resolution measurements by SAMPEX of the precipitation of relativistic electrons, *Adv. Space Res.*, *18*(8), 171–186.
- Berthelier, J. J., et al. (2006), ICE: The electric field experiment on DEMETER, *Planet. Space Sci.*, *54*(5), 456–471.
- Borovsky, J. E., R. J. Nemzek, and R. D. Belian (1993), The occurrence rate of magnetospheric-substorm onsets: Random and periodic substorms, *J. Geophys. Res.*, *98*(A3), 3807–3813, doi:10.1029/92JA02556.
- Bortnik, J., and R. M. Thorne (2007), The dual role of ELF/VLF chorus waves in the acceleration and precipitation of radiation belt electrons, *J. Atmos. Sol. Terr. Phys.*, *69*, 378–386.
- Choudhuri, A. R., P. Chatterjee, and J. Jiang (2007), Predicting solar cycle 24 with a solar dynamo model, *Phys. Rev. Lett.*, *98*, 131103.
- Clilverd, M. A., E. Clarke, T. Ulich, H. Rishbeth, and M. J. Jarvis (2006), Predicting solar cycle 24 and beyond, *Space Weather*, *4*, S09005, doi:10.1029/2005SW000207.
- Cresswell-Moorcock, K., C. J. Rodger, A. Kero, A. B. Collier, M. A. Clilverd, I. Häggström, and T. Pitkänen (2013), A reexamination of latitudinal limits of substorm-produced energetic electron precipitation, *J. Geophys. Res. Space Physics*, *118*, 6694–6705, doi:10.1002/jgra.50598.
- Cresswell-Moorcock, K., C. J. Rodger, M. A. Clilverd, and D. K. Milling (2015), Techniques to determine the quiet day curve for a long period of subionospheric VLF observations, *Radio Sci.*, *50*, 453–468, doi:10.1002/2015RS005652.
- Dikpati, M., G. de Toma, and P. A. Gilman (2006), Predicting the strength of solar cycle 24 using a flux-transport dynamo-based tool, *Geophys. Res. Lett.*, *33*, L05102, doi:10.1029/2005GL025221.
- Evans, D. S., and M. S. Greer (2004), Polar Orbiting Environmental Satellite space environment monitor—2: Instrument descriptions and archive data documentation, NOAA technical Memorandum version 1.4, Space Environment Laboratory, Colo.
- Gibson, S. E., et al. (2011), The whole heliosphere interval in the context of a long and structured solar minimum: An overview from Sun to Earth, *Sol. Phys.*, *274*, 5–27.
- Gjerloev, J. W. (2012), The SuperMAG data processing technique, *J. Geophys. Res.*, *117*, A09213, doi:10.1029/2012JA017683.
- Hathaway, D. H., and R. M. Wilson (2006), Geomagnetic activity indicates large amplitude for sunspot cycle 24, *Geophys. Res. Lett.*, *33*, L18101, doi:10.1029/2006GL027053.
- Kepko, L., H. E. Spence, and H. J. Singer (2002), ULF waves in the solar wind as direct drivers of magnetospheric pulsations, *Geophys. Res. Lett.*, *29*(8), 1197, doi:10.1029/2001GL014405.
- Kilpua, E. K. J., J. G. Luhmann, L. K. Jian, C. T. Russell, and Y. Li (2014), Why have geomagnetic storms been so weak during the recent solar minimum and the rising phase of cycle 24?, *J. Atmos. Sol. Terr. Phys.*, *107*, 12–19, doi:10.1016/j.jastp.2013.11.001.
- Kissinger, J., L. Kepko, D. N. Baker, S. Kanekal, W. Li, R. L. McPherron, and V. Angelopoulos (2014), The importance of storm time steady magnetospheric convection in determining the final relativistic electron flux level, *J. Geophys. Res. Space Physics*, *119*, 7433–7443, doi:10.1002/2014JA019948.
- Klecker, B., et al. (1993), HILT: A heavy ion large area proportional counter telescope for solar and anomalous cosmic rays, *IEEE Trans. Geosci. Remote Sens.*, *31*(3), 542–548, doi:10.1109/36.225520.
- Kullen, A., and T. Karlsson (2004), On the relation between solar wind, pseudobreakups, and substorms, *J. Geophys. Res.*, *109*, A12218, doi:10.1029/2004JA010488.
- Lam, M. M., R. B. Horne, N. P. Meredith, S. A. Glauert, T. Moffat-Griffin, and J. C. Green (2010), Origin of energetic electron precipitation >30 keV into the atmosphere, *J. Geophys. Res.*, *115*, A00F08, doi:10.1029/2009JA014619.
- Lave, K. A., et al. (2013), Elemental GCR observations during the 2009–2010 solar minimum period, *NASA Tech. Rep.*, GSFC-E-DA-TN10268.
- Li, X., and M. Temerin (2001), The electron radiation belt, *Space Sci. Rev.*, *95*(1–2), 569–580, doi:10.1023/A:1005221108016.
- Li, X., D. N. Baker, M. Temerin, D. Larson, R. P. Lin, G. D. Reeves, M. Looper, S. G. Kanekal, and R. A. Mewaldt (1997), Are energetic electrons in the solar wind the source of the outer radiation belt?, *Geophys. Res. Lett.*, *24*(8), 923–926, doi:10.1029/97GL00543.
- Lyons, L. R., D.-Y. Lee, R. M. Thorne, R. B. Horne, and A. J. Smith (2005), Solar wind-magnetosphere coupling leading to relativistic electron energization during high-speed streams, *J. Geophys. Res.*, *110*, A11202, doi:10.1029/2005JA011254.
- Mauk, B. H., N. J. Fox, S. G. Kanekal, R. L. Kessel, D. G. Sibeck, and A. Ukhorskiy (2013), Science objectives and rationale for the Radiation Belt Storm Probes mission, *Space Sci. Rev.*, *179*, 3–27, doi:10.1007/s11214-012-9941-x.
- McDonald, F. B., W. R. Webber, and D. V. Reames (2010), Unusual time histories of galactic and anomalous cosmic rays at 1 AU over the deep solar minimum of cycle 23/24, *Geophys. Res. Lett.*, *37*, L18101, doi:10.1029/2010GL044218.

- McPherron, R. L., D. N. Baker, and N. U. Crooker (2009), Role of the Russell-McPherron effect in the acceleration of relativistic electrons, *J. Atmos. Sol. Terr. Phys.*, *71*, 1032–1044.
- Meredith, N. P., R. B. Horne, R. H. A. Iles, R. M. Thorne, D. Heynderickx, and R. R. Anderson (2002), Outer zone relativistic electron acceleration associated with substorm-enhanced whistler mode chorus, *J. Geophys. Res.*, *107*(A7), 1144, doi:10.1029/2001JA900146.
- Meredith, N. P., M. Cain, R. B. Horne, R. M. Thorne, D. Summers, and R. R. Anderson (2003), Evidence for chorus-driven electron acceleration to relativistic energies from a survey of geomagnetically disturbed periods, *J. Geophys. Res.*, *108*(A6), 1248, doi:10.1029/2002JA009764.
- Meredith, N. P., R. B. Horne, R. M. Thorne, D. Summers, and R. R. Anderson (2004), Substorm dependence of plasmaspheric hiss, *J. Geophys. Res.*, *109*, A06209, doi:10.1029/2004JA010387.
- Millan, R. M., and D. N. Baker (2012), Acceleration of particles to high energies in Earth's radiation belts, *Space Sci. Rev.*, *173*, 103–131, doi:10.1007/s11214-012-9908-y.
- Miyoshi, Y., and R. Kataoka (2008), Flux enhancement of the outer radiation belt electrons after the arrival of stream interaction regions, *J. Geophys. Res.*, *113*, A03S09, doi:10.1029/2007JA012506.
- Miyoshi, Y., R. Kataoka, Y. Kasahara, A. Kumamoto, T. Nagai, and M. F. Thomsen (2013), High-speed solar wind with southward interplanetary magnetic field causes relativistic electron flux enhancement of the outer radiation belt via enhanced condition of whistler waves, *Geophys. Res. Lett.*, *40*, 4520–4525, doi:10.1002/grl.50916.
- Morley, S. K., A. P. Rouillard, and M. P. Freeman (2009), Recurrent substorm activity during the passage of a corotating interaction region, *J. Atmos. Sol. Terr. Phys.*, *71*(10–11), 1073.
- Morley, S. K., R. H. W. Friedel, E. L. Spanswick, G. D. Reeves, J. T. Steinberg, J. Koller, T. Cayton, and E. Noveroske (2010), Dropouts of the outer electron radiation belt in response to solar wind stream interfaces: Global Positioning System observations, *Proc. R. Soc. A*, *466*(2123), 3329, doi:10.1098/rspa.2010.0078.
- Nakamura, R., K. Kamei, and Y. Kamide (1998), SAMPEX observations of storm-associated electron flux variations in the outer radiation belt, *J. Geophys. Res.*, *103*(A11), 26,261–26,269, doi:10.1029/97JA02873.
- Neal, J. J., C. J. Rodger, M. A. Clilverd, N. R. Thomson, T. Raita, and T. Ulich (2015), Long-term determination of energetic electron precipitation into the atmosphere from AARDDVARK subionospheric VLF observations, *J. Geophys. Res. Space Physics*, *120*, 2194–2211, doi:10.1002/2014JA020689.
- Newell, P. T., and J. W. Gjerloev (2011a), Evaluation of SuperMAG auroral electrojet indices as indicators of substorms and auroral power, *J. Geophys. Res.*, *116*, A12211, doi:10.1029/2011JA016779.
- Newell, P. T., and J. W. Gjerloev (2011b), Substorm and magnetosphere characteristic scales inferred from the SuperMAG auroral electrojet indices, *J. Geophys. Res.*, *116*, A12232, doi:10.1029/2011JA016936.
- Paulikas, G. A., and J. B. Blake (1979), Effects of the solar wind on magnetospheric dynamics: Energetic electrons at the synchronous orbit, in *Quantitative Modeling of Magnetospheric Processes, Geophys. Monogr. Ser.*, vol. 21, edited by W. P. Olson, pp. 180–202, AGU, Washington, D. C.
- Pokhotelov, D., I. J. Rae, K. R. Murphy, and I. R. Mann (2015), The influence of solar wind variability on magnetospheric ULF wave power, *Ann. Geophys.*, *33*, 697–701, doi:10.5194/angeo-33-697-2015.
- Pulkkinen, T. I., N. Partamies, and E. K. J. Kilpua (2014), Substorm occurrence during quiet solar wind driving, *J. Geophys. Res. Space Physics*, *119*, 2978–2989, doi:10.1002/2013JA019503.
- Reeves, G. D., S. K. Morley, R. H. W. Friedel, M. G. Henderson, T. E. Cayton, G. Cunningham, J. B. Blake, R. A. Christensen, and D. Thomsen (2011), On the relationship between relativistic electron flux and solar wind velocity: Paulikas and Blake revisited, *J. Geophys. Res.*, *116*, A02213, doi:10.1029/2010JA015735.
- Reeves, G. D., et al. (2013), Electron acceleration in the heart of the Van Allen radiation belts, *Science*, *341*, 991–994, doi:10.1126/science.1237743.
- Reeves, G., A. Chan, and C. J. Rodger (2009), New directions for radiation belt research, *Space Weather*, *7*, S07004, doi:10.1029/2008SW000436.
- Reeves, G., S. Morley, and G. Cunningham (2013), Long-term variations in solar wind velocity and radiation belt electrons, *J. Geophys. Res. Space Physics*, *118*, 1040–1048, doi:10.1002/jgra.50126.
- Rodger, C. J., B. R. Carson, S. A. Cummer, R. J. Gamble, M. A. Clilverd, J. C. Green, J.-A. Sauvaud, M. Parrot, and J.-J. Berthelier (2010a), Contrasting the efficiency of radiation belt losses caused by ducted and nonducted whistler-mode waves from ground-based transmitters, *J. Geophys. Res.*, *115*, A12208, doi:10.1029/2010JA015880.
- Rodger, C. J., M. A. Clilverd, J. C. Green, and M. M. Lam (2010b), Use of POES SEM-2 observations to examine radiation belt dynamics and energetic electron precipitation into the atmosphere, *J. Geophys. Res.*, *115*, A04202, doi:10.1029/2008JA014023.
- Rodger, C. J., A. J. Kavanagh, M. A. Clilverd, and S. R. Marple (2013), Comparison between POES energetic electron precipitation observations and riometer absorptions: Implications for determining true precipitation fluxes, *J. Geophys. Res. Space Physics*, *118*, 7810–7821, doi:10.1002/2013JA019439.
- Russell, C. T., J. G. Luhmann, and L. K. Jian (2010), How unprecedented a solar minimum?, *Rev. Geophys.*, *48*, RG2004, doi:10.1029/2009RG000316.
- Svalgaard, L., E. W. Cliver, and Y. Kamide (2005), Sunspot cycle 24: Smallest cycle in 100 years?, *Geophys. Res. Lett.*, *32*, L01104, doi:10.1029/2004GL021664.
- Thomsen, M. F. (2004), Why K_p is such a good measure of magnetospheric convection, *Space Weather*, *2*, S11004, doi:10.1029/2004SW000089.
- Thorne, R. M. (2010), Radiation belt dynamics: The importance of wave-particle interactions, *Geophys. Res. Lett.*, *37*, L22107, doi:10.1029/2010GL044990.
- Tsurutani, B. T., and E. J. Smith (1974), Postmidnight chorus: A substorm phenomenon, *J. Geophys. Res.*, *79*(1), 118–127, doi:10.1029/JA079i001p00118.
- Walach, M.-T., and S. E. Milan (2015), Are steady magnetospheric convection events prolonged substorms?, *J. Geophys. Res. Space Physics*, *120*, 1751–1758, doi:10.1002/2014JA020631.
- Weimer, D. R. (1994), Substorm time constants, *J. Geophys. Res.*, *99*(A6), 11,005–11,015, doi:10.1029/93JA02721.
- Whittaker, I. C., C. J. Rodger, M. A. Clilverd, and J.-A. Sauvaud (2014), The effects and correction of the geometric factor for the POES/MEPED electron flux instrument using a multisatellite comparison, *J. Geophys. Res. Space Physics*, *119*, 6386–6404, doi:10.1002/2014JA020021.
- Yando, K., R. M. Millan, J. C. Green, and D. S. Evans (2011), A Monte Carlo simulation of the NOAA POES medium energy proton and electron detector instrument, *J. Geophys. Res.*, *116*, A10231, doi:10.1029/2011JA016671.
- Zhao, L.-L., G. Qin, M. Zhang, and B. Heber (2014), Modulation of galactic cosmic rays during the unusual solar minimum between cycles 23 and 24, *J. Geophys. Res. Space Physics*, *119*, 1493–1506, doi:10.1002/2013JA019550.